Chinese Chemical Letters 36 (2025) 109865

Contents lists available at ScienceDirect

Chinese Chemical Letters

journal homepage: www.elsevier.com/locate/cclet

Self-assembly of two pairs of homochiral M_2L_4 coordination capsules with varied confined space using Tröger's base ligands

Yi Zhou[a], Wei Zhang[a], Rong Fu[a], Jiaxin Dong[a], Yuxuan Liu[a], Zihang Song[a], Han Han[b,c,*], Kang Cai[a,*]

[a] College of Chemistry, Nankai University, Tianjin 300071, China
[b] Department of Chemistry, Northwestern University, Evanston, IL 60208, United States
[c] Department of Chemistry, The University of Hong Kong, Hong Kong SAR 999077, China

ARTICLE INFO

Article history:
Received 20 January 2024
Revised 26 March 2024
Accepted 7 April 2024
Available online 9 April 2024

Keywords:
Metal-organic capsule
Chirality
Self-sorting
Tröger's base
Host-guest recognition

ABSTRACT

Chiral coordination molecular cages/capsules with discrete nanoconfined chiral cavities demonstrate significant potential applications across various fields. In this study, we utilized Tröger's base as the building block to design and synthesize two pairs of enantiopure ligands. These ligands were then self-assembled with Pd(II) ions through chiral self-sorting coordination, resulting in the formation of two pairs of homochiral M_2L_4-type coordination molecular capsules. Notably, due to differences in the substitution positions on the Tröger's base, these two pairs of enantiomeric coordination molecular capsules exhibited distinct levels of cavity closures, cavity sizes, and host-guest recognition properties. This research offers valuable insights into the construction of novel chiral molecular capsules and the regulation of confined cavities.

Metal-organic cages/capsules (MOCs) based on coordination interactions have long been a focal point in supramolecular chemistry and related fields due to their modular constructions, thermodynamically driven quantitative self-assembly and confined cavity environments [1–10]. The introduction of chiral ligands enables the preparation of chiral MOCs, whose chiral cavity environments are useful for applications like chiral molecule recognition [11–14], chiral separation [15,16], and asymmetric catalysis [17–19]. Consequently, the construction and study of chiral MOCs have garnered increasing attention [20–22]. However, challenges in building chiral MOCs and functional research persist considering limited types of chiral building blocks and difficulties in obtaining enantiopure ligands.

As a chiral organic base, Tröger's base (TB) can be synthesized *via* a one-step condensation between aromatic amines and formaldehyde [23]. Notably, Belowich *et al.* have demonstrated that enantiopure TB derivatives can be conveniently obtained through crystallization-induced asymmetric transformation (CIAT) utilizing dibenzoyl-tartaric acid (DBTA) [24]. Moreover, TB's *V*-shaped, inward-bending conformation make it particularly suited for constructing MOCs with aromatic shells. In contrast to MOCs with wirelike frameworks [25], MOCs featuring aromatic shells [26–33] offer more favorable noncovalent interactions and a stronger solvophobic effect, thereby providing advantages for guest-encapsulation. Thus, we believe TB is an ideal molecular building block for constructing chiral MOCs, a potential that has, however, been rarely explored [34].

Herein, we used enantiopure TB as the building block and synthesized two TB-based pyridine ligands, **L1** and **L2**, through substitution at different positions on TB. Inspired by Clever *et al.* [35,36], **L1** and **L2** were further coordinated with Pd(II) to form two homochiral M_2L_4-type MOCs, namely, **MOC-1** and **MOC-2** (Fig. 1). It is noteworthy that self-sorting assembly occurred with racemic ligands *RR*-**L1** and *SS*-**L1**, forming homochiral capsules R_8-**MOC-1** and S_8-**MOC-1**, while a mixture of two different ligands also leaded to narcissistic self-sorting, producing **MOC-1** and **MOC-2**, respectively. Crystallographic analysis revealed that the substitution differences on TB resulted in MOCs with varied cavity sizes and closure extents. Significantly, the fully enclosed cavity of **MOC-1** was capable of encapsulating one [2.2]paracyclophane (PCP) guest to form a stable 1:1 complex with slow exchange kinetics on the ^{1}H NMR timescale. These findings provide insights for the establishment of novel chiral molecular capsules and the control of confined cavities.

Tröger's base ligands **L1** and **L2** were synthesized through one-step Suzuki coupling, initiated from their enantiopure precursors **1** and **2**, along with pyridine derivatives (Scheme 1). The synthetic

* Corresponding authors.
E-mail addresses: hanhan23@hku.hk (H. Han), kangcai@nankai.edu.cn (K. Cai).

https://doi.org/10.1016/j.cclet.2024.109865
1001-8417/

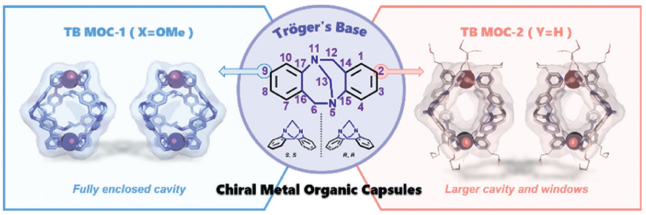

Fig. 1. The design of chiral metal organic capsules using Tröger's base ligands.

routes for precursors **1** and **2** and their chiral resolutions based on CIAT strategy are elaborated in Schemes S1 and S2 (Supporting information). **L1** is characterized by a methoxy group at positions 2 and 8 in the Tröger's base skeleton, while **L2** features modification on the pyridine ring with a pendant methoxyethoxy chain to enhance the solubility. Upon reacting enantiopure **L1** or **L2** with $Pd(CH_3CN)_4(BF_4)_2$ at a molar ratio of 1:0.6 in CD_3CN at 80 °C for 3 h, a clear and colorless solution was obtained, followed by the precipitation of the corresponding chiral **MOC-1** or **MOC-2** as a white powder after the addition of diethyl ether. Significant shifts of several resonances in the ^1H NMR spectrum of S_8-**MOC-1**, were observed when compared to ligand **L1** (Figs. 2a and b), suggesting the coordination of pyridine to Pd(II). The proton 1 associated with pyridine units displayed an upfield shift due to shielding effect within the capsule's cavity. The other protons, influenced by the electron-withdrawing effect of Pd(II), exhibited downfield shifts. Similar spectral characteristics were observed for S_8-**MOC-2** (Figs. 2d and e), suggesting the quantitative formation of a single compound with high symmetry derived from the complexation of the ligand with Pd(II). Consistently, diffusion-ordered ^1H NMR spectroscopy (DOSY) corroborated this by showing uniform diffusion coefficients $D = 5.248 \times 10^{-10}$ m^2/s for all protons in S_8-**MOC-1**, which, according to the Stocks-Einstein equation, indicated a radius size of 11.53 Å (Fig. 2c, Figs. S39 and S40 in Supporting information). Similarly, the DOSY spectrum of S_8-**MOC-2** showed a single band with a diffusion coefficient $D = 4.898 \times 10^{-10}$ m^2/s, yielding a calculated radius of 12.33 Å in line with the ligand length (Fig. 2f, Figs. S41 and S42 in Supporting information).

Additionally, the enantiomers of both homochiral capsules were characterized using circular dichroism (CD) spectroscopy, exhibiting perfect mirror-image CD signals (Fig. 3). Comprehensive analysis of the CD and UV–vis spectra revealed strong Cotton effects for R_8-**MOC-1** at 290 nm (positive) and 340 nm (positive), while the enantiomer S_8-**MOC-1** demonstrates opposite Cotton effects at the same wavelengths. Similarly, the enantiomers of **MOC-2** exhibited strong Cotton effects at 254, 266, 290 and 333 nm.

Conclusive evidence for the formation of M_2L_4 homochiral capsules was obtained from their single-crystal structures. By slow evaporation of diisopropyl ether into acetonitrile solutions of the capsules, single crystals of S_8-**MOC-1** (Fig. 4a) and S_8-**MOC-2** (Fig. 4b) were obtained. Both crystal structures contained two Pd^{2+} ions respectively, each in a square planar N_4 coordination environment, bridged by four ligands with electron-rich aromatic rings forming the capsule shells. In S_8-**MOC-1**, the distance between two Pd^{2+} ions was 11.05 Å, slightly shorter than that (11.12 Å) in S_8-**MOC-2**. This difference can be attributed to varied substitution sites on the TB skeletons. The directional nature of the Tröger's base backbone leaded to twisted capsule shells, yet maintained an overall orientation around a C_4-symmetry axel. While the structures were expected to display high symmetry, their symmetry was slightly reduced on account of substitution effect. S_8-**MOC-1** belonged to tetragonal *I*422 chiral space group, while S_8-**MOC-2** was assigned to *P*1 space group, influenced by its more flexible pendant hydrophilic chain. Notably, the pyridine segment at different connecting sites on TB resulted in two ligands exhibiting different tilt angles when coordinating with Pd(II), leading to the formation of two MOCs with distinct cavity sizes and different closure degrees for the confined spaces. As indicated by MoloVol software calculations [37], S_8-**MOC-1** and S_8-**MOC-2** displayed cavity volumes of 280 $Å^3$ and 382 $Å^3$, respectively. Besides, S_8-**MOC-1**′s cavity was devoid of counterions, whereas S_8-**MOC-2**′s cavity encapsulated a counterion (BF_4^-) and several solvent molecules (Fig. S44 in Supporting information). Moreover, due to the larger tilt angle of the ligands and the presence of methoxy groups, S_8-**MOC-1** formed a fully enclosed capsule as depicted in surface overlay images, while S_8-**MOC-2** displayed four narrow open windows with widths of *ca.* 3.5 Å.

We subsequently explored the chiral self-sorting assembly behaviors using racemic ligands *RR*-**L1** and *SS*-**L1** to coordinate with Pd(II). The ^1H NMR spectra only displayed a single set of signals, indicating that enantiomeric ligands undergo self-recognition to form homochiral capsules R_8-**MOC-1** and S_8-**MOC-1** (Figs. S46-S48 in Supporting information), instead of the occurrence of social or comprehensive self-sorting. To evaluate the influence of non-covalent interactions on ligand bending angles, additional self-

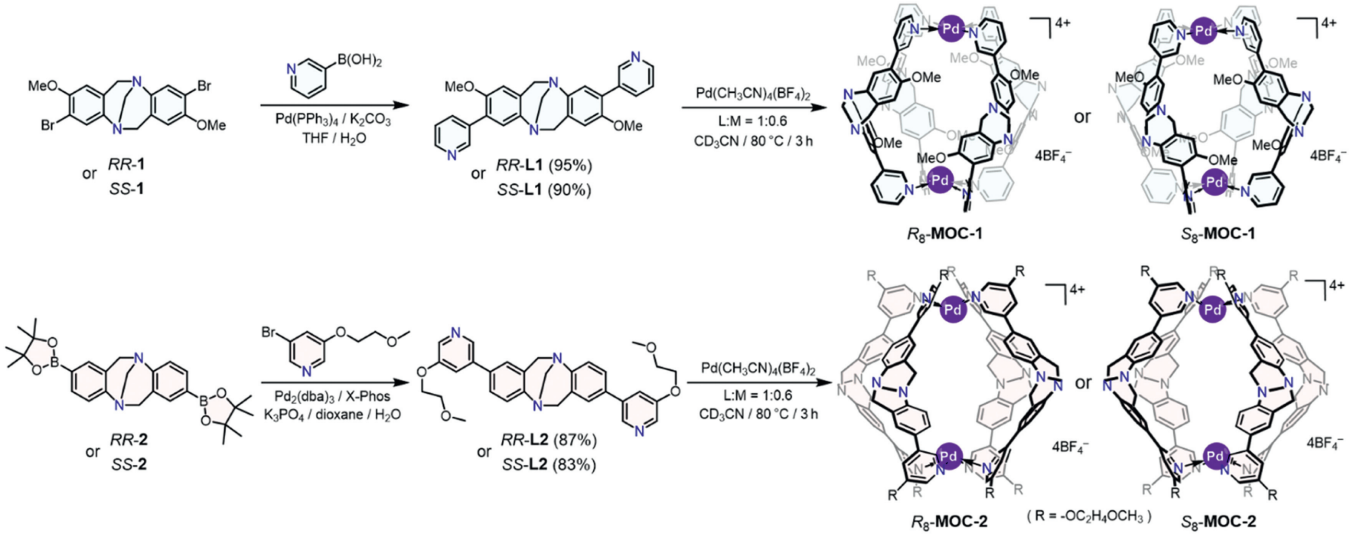

Scheme 1. The synthetic routes of homochiral Tröger's base metal-organic capsules **MOC-1** and **MOC-2**.

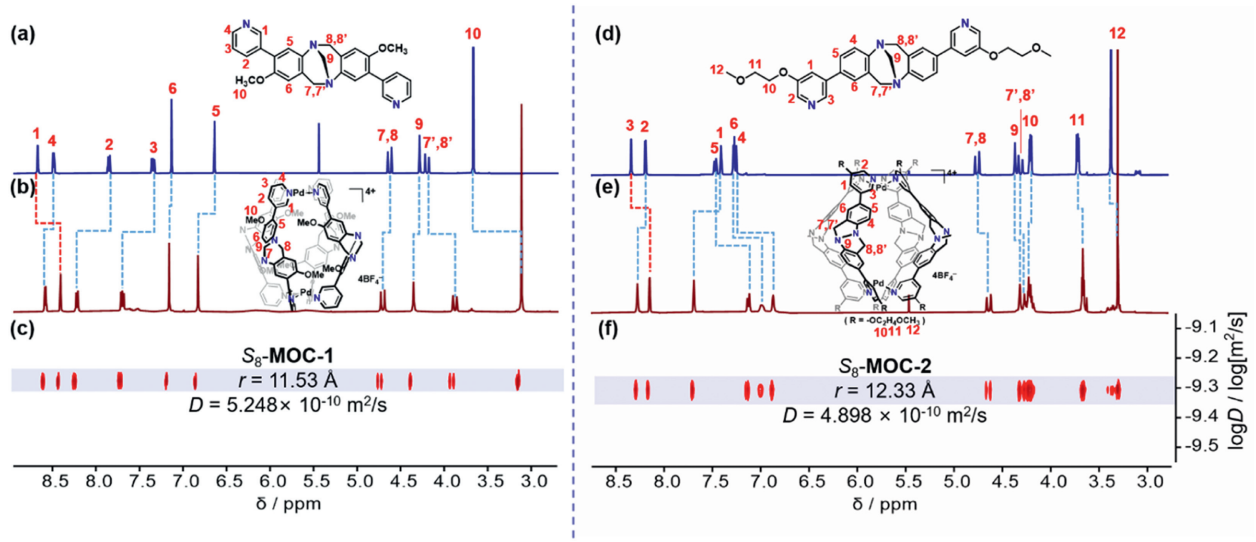

Fig. 2. ^{1}H NMR spectra (400 MHz, CD_3CN, 298 K) of (a) *SS*-**L1** and (b) its self-assembly product S_8-**MOC-1**. (c) DOSY spectrum of S_8-**MOC-1**. ^{1}H NMR spectra (400 MHz, CD_3CN, 298 K) of (d) *SS*-**L2** and (e) S_8-**MOC-2**. (f) DOSY spectrum of S_8-**MOC-2**.

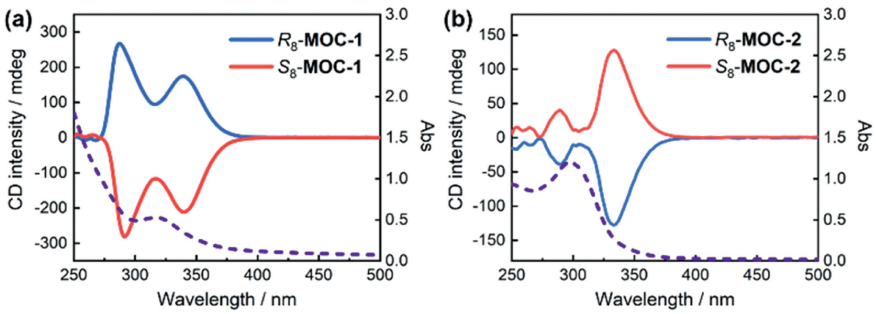

Fig. 3. Circular dichroism (CH_3CN, 0.10 mmol/L for **MOC-1**, 50 μmol/L for **MOC-2**, 298 K) and UV–vis spectra (CH_3CN, 10 μmol/L, 298 K) of (a) **MOC-1** and (b) **MOC-2**.

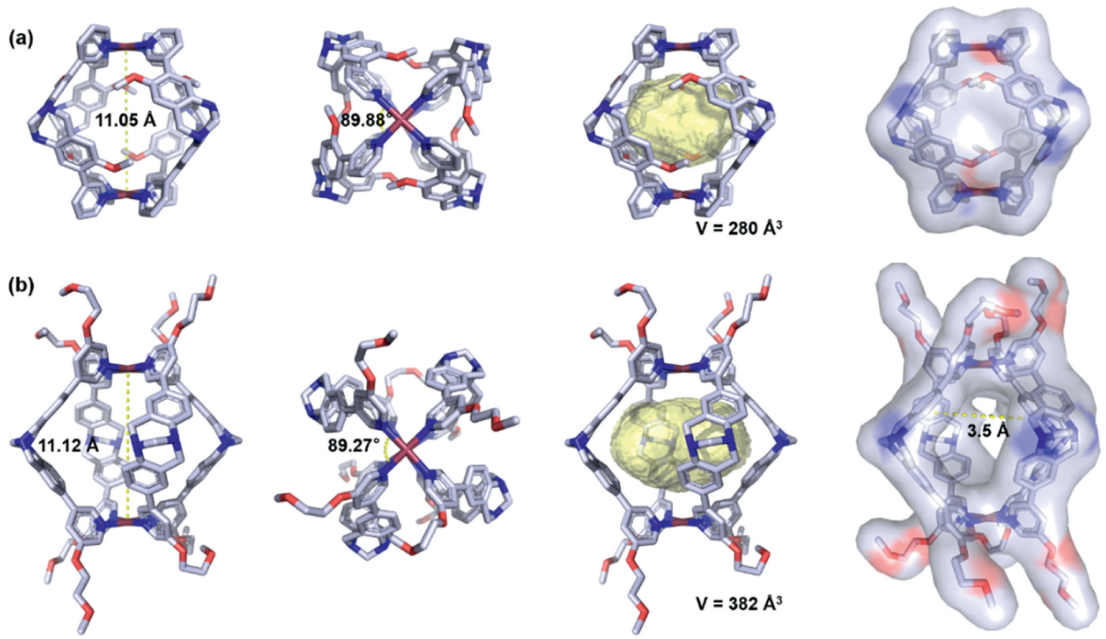

Fig. 4. Single-crystal structures and cavity volume calculations of (a) S_8-**MOC-1** and (b) S_8-**MOC-2**. The figures present, from left to right, side-on and top-down views of capsules illustrated as stick representations, side-on views of the cavity conformation as calculated by MoloVol software, and the surface representation superimposed. Hydrogen atoms, BF_4^- counterions and solvent molecules have been omitted for the sake of clarity.

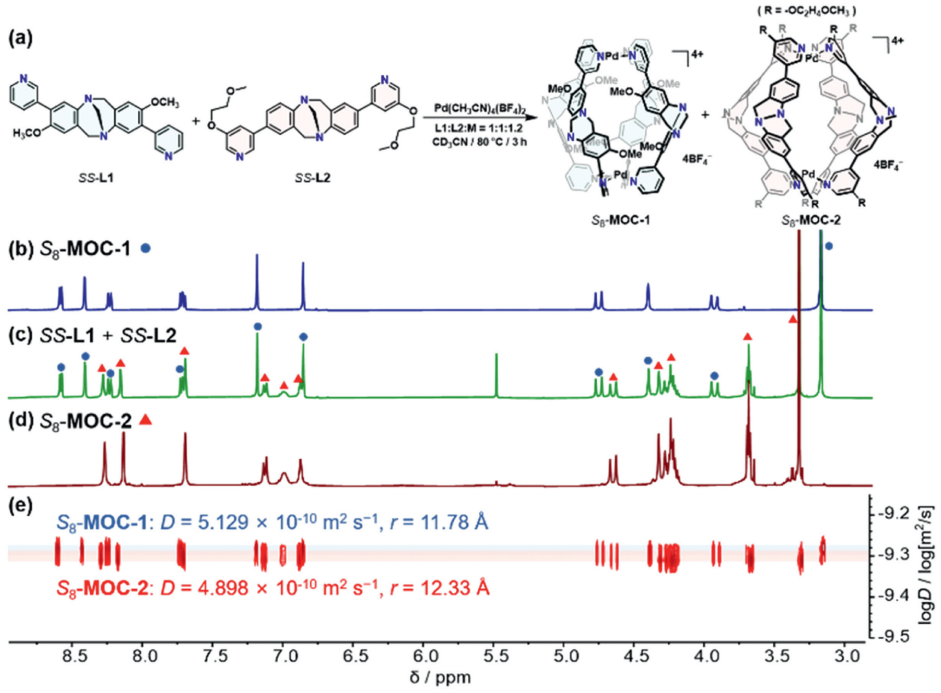

Fig. 5. (a) Narcissistic self-sorting of S_8-**MOC-1** and S_8-**MOC-2** capsules from mixed ligands. ^{1}H NMR spectra (400 MHz, CD_3CN, 298 K) of (b) S_8-**MOC-1** and (d) S_8-**MOC-2**. (c) ^{1}H NMR spectra and (e) DOSY spectra (400 MHz, CD_3CN, 298 K) illustrating the self-sorting outcomes with a mixture of S_8-**MOC-1** and S_8-**MOC-2** species.

sorting studies involving different ligands were also conducted. Theoretical analysis suggested that two Tröger's base ligands with similar backbones might achieve similar bending angles, potentially leading to heteroleptic structures containing both **L1** and **L2** [38,39]. However, the formation of heteroleptic capsule was found to be unfavorable when an equimolar *SS*-**L1** and *SS*-**L2** were mixed with $Pd(CH_3CN)_4(BF_4)_2$ in CD_3CN (Fig. 5a). The ^{1}H NMR spectra revealed two clear sets of signals corresponding to compounds S_8-**MOC-1** and S_8-**MOC-2** (Figs. 5b-d). Additionally, the DOSY spectra also showed two distinct bands corresponding to the smaller-radius **MOC-1** and the larger-radius **MOC-2**, despite being closely spaced (Fig. 5e). Comparable results were observed using ligands *RR*-**L1** and *SS*-**L2** with opposite chirality (Figs. S52-S54 in Supporting information). These results demonstrated that narcissistic self-sorting had occurred.

The variances in sizes and closure extents of the cavities in **MOC-1** and **MOC-2** also resulted in distinct host-guest recognition properties. **MOC-1** was capable of recognizing a size-matched guest, [2.2]paracyclophane (PCP, molecular volume: 198 Å^3), while **MOC-2** was not. Upon suspending PCP (0.70 equiv. relative to S_8-**MOC-1**) in a 2.0 mmol/L CD_3CN solution of S_8-**MOC-1** at 80 °C overnight, a white suspension was obtained. In the ^{1}H NMR spectrum (Fig. 6b), there were four distinct sets of peaks. Two sets of resonances corresponded unequivocally to the unbound S_8-**MOC-1** (Fig. 6a, blue circles) and the free guest PCP (Fig. 6c, red triangles), while the other two were notably shifted compared with those associated with the free host and guest, suggesting the formation of host-guest complexes. These results indicated that the unbound capsule, free guest, and host-guest complexes coexisted in the solution, with the host-guest binding process featuring slow exchange kinetics on the ^{1}H NMR timescale. Compared to free PCP, the protons in the encapsulated guest displayed considerable upfield shift ($\Delta\delta > 1.4$ ppm) due to shielding effect inside the cavity, with methylene protons b separated into two sets of peaks. Further, the calculation of integral area determined 1:1 binding between the host and guest (Fig. S55 in Supporting information), revealing a binding constant of 5.0×10^3 L/mol. The formation of the host-guest complex was further substantiated by the DOSY spectra (Fig. S56 in Supporting information). Spatial correlation signals were observed between the aromatic peak ($H_{a'}$) of the bound guest and the pyridine proton peak (H_1) that was oriented towards the interior of the cavity, as evidenced in the ROESY spectrum (Fig. S57 in Supporting information). Furthermore, the structure of the host-guest complex was optimized using the GFN2-xTB calculation method (Fig. S58 in Supporting information) [40]. Rebek's investigations elucidate that optimal binding is attained when the guest molecule's dimensions match precisely with the inner cavity of the capsule, with the packing coefficient reaching an ideal value of approximately 55%. Despite the substantial volume of PCP, which poses a theoretical encapsulation challenge within S_8-**MOC-1**, we observed a remarkable 1:1 binding efficiency, accompanied by a packing coefficient of 71%. This intriguing outcome is presumably facilitated by intermolecular forces, including [C–H$\cdots\pi$] and [$\pi\cdots\pi$] interactions, during the encapsulation process. These forces impart enhanced stability to the host-guest complex, thereby accommodating the encapsulation of guest molecules with larger volumes.

In summary, two enantiopure Tröger's base ligands have been designed and self-assembled with Pd(II) to form two M_2L_4-type chiral metal-organic capsules. Differences in substitution sites on the TB's backbone resulted in varied sizes and closure degrees of the confined cavities in **MOC-1** and **MOC-2**. Single crystal X-ray analysis of the two *S*-configured homochiral capsules revealed cavity volumes of 280 Å^3 and 382 Å^3 for **MOC-1** and **MOC-2**, respectively. Narcissistic chiral self-sorting occurred when mixing two racemic chiral ligands for coordination. The fully enclosed capsule **MOC-1** was able to encapsulate one [2.2]paracyclophane guest to form a stable 1:1 host-guest complex with slow exchange kinetics on the ^{1}H NMR timescale, while **MOC-2**, featuring a larger cavity and open windows, was incapable of encapsulating this guest. This research offers valuable insight into the construction of novel chiral molecular capsules and the control of confined cavities. More comprehensive investigation of the host-guest recognition capabilities for both MOCs, particularly regarding the potential application

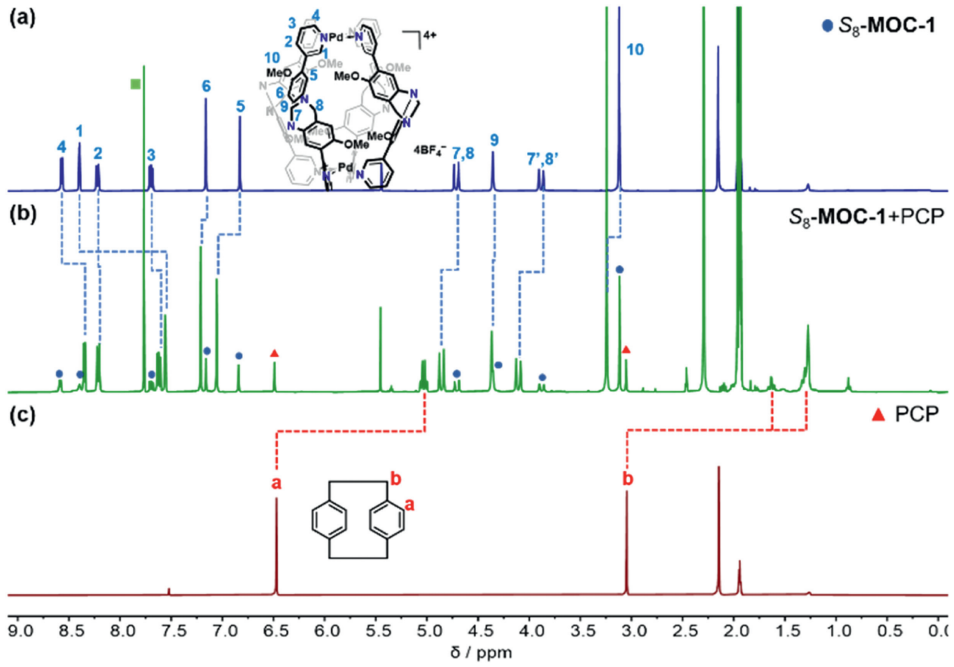

Fig. 6. ^{1}H NMR spectra (400 MHz, CD_3CN, 298 K) of (a) S_8-**MOC-1** (5.00 mmol/L). (b) A mixture of S_8-**MOC-1** (2.22 mmol/L) and [2.2]paracyclophane (PCP) (1.56 mmol/L) with a molar ratio of 1.0:0.70, (c) free PCP (10.0 mmol/L).

of the chiral cavities in differentiation [41] and separation [42] of chiral guests, is a promising avenue for future exploration.

Declaration of competing interest

The authors declare that they have no known competing financial interests or personal relationships that could have appeared to influence the work reported in this paper.

CRediT authorship contribution statement

Yi Zhou: Data curation, Formal analysis, Investigation, Methodology, Project administration, Validation, Visualization, Writing – original draft. **Wei Zhang:** Formal analysis, Methodology, Writing – review & editing. **Rong Fu:** Software, Validation. **Jiaxin Dong:** Investigation, Validation. **Yuxuan Liu:** Investigation. **Zihang Song:** Methodology. **Han Han:** Formal analysis, Resources, Writing – review & editing. **Kang Cai:** Conceptualization, Project administration, Resources, Supervision, Writing – review & editing.

Acknowledgments

This work is supported by the National Natural Science Foundation of China (No. 22271164), the Fundamental Research Funds for the Central Universities and Nankai University (NKU). This work also made use of the IMSERC at Northwestern University, which has received support from the State of Illinois and International Institute for Nanotechnology (IIN).

During the preparation of this work, the authors used GPT in order to polish the language. After using this tool, the authors reviewed and edited the content as needed and take full responsibility for the content of the publication.

Supplementary materials

Supplementary material associated with this article can be found, in the online version, at doi:10.1016/j.cclet.2024.109865.

References

[1] C.L. Liu, E.O. Bobylev, S. Dauriac, et al., CCS Chem. 5 (2023) 1–31.
[2] Y. Li, J. Dong, W. Gong, et al., J. Am. Chem. Soc. 143 (2021) 20939–20951.
[3] Y.P. Wang, Y. Zhang, X.H. Duan, et al., Coord. Chem. Rev. 501 (2024) 215570.
[4] S. Pullen, J. Tessarolo, G.H. Clever, Chem. Sci. 12 (2021) 7269–7293.
[5] A. Walther, I. Regeni, J.J. Holstein, G.H. Clever, J. Am. Chem. Soc. 145 (2023) 25365–25371.
[6] J. Gemen, J.R. Church, T.P. Ruoko, et al., Science 381 (2023) 1357–1363.
[7] D. Zhang, T.K. Ronson, Y.Q. Zou, J.R. Nitschke, Nat. Rev. Chem. 5 (2021) 168–182.
[8] R. Banerjee, D. Chakraborty, P.S. Mukherjee, J. Am. Chem. Soc. 145 (2023) 7692–7711.
[9] S.P. Zheng, Y.W. Xu, P.Y. Su, et al., Chin. Chem. Lett. 35 (2024) 108477.
[10] Z.X. Lian, X.Z. Wang, C.W. Zhou, et al., Chin. Chem. Lett. 35 (2024) 109063.
[11] G. Wu, Y. Chen, S. Fang, et al., Angew. Chem. Int. Ed. 60 (2021) 16594–16599.
[12] Y.H. Huang, Y.L. Lu, X.D. Zhang, et al., Angew. Chem. Int. Ed. 63 (2024) e202315053.
[13] G. Li, T.K. Ronson, R. Lavendomme, et al., Chem 9 (2023) 1549–1561.
[14] S.J. Hu, X.Q. Guo, L.P. Zhou, et al., J. Am. Chem. Soc. 144 (2022) 4244–4253.
[15] W. Xue, L. Pesce, A. Bellamkonda, et al., J. Am. Chem. Soc. 145 (2023) 5570–5577.
[16] Y.J. Hou, K. Wu, Z.W. Wei, et al., J. Am. Chem. Soc. 140 (2018) 18183–18191.
[17] J.S. Wang, K. Wu, C. Yin, et al., Nat. Commun. 11 (2020) 4675.
[18] K. Li, K. Wu, Y.L. Lu, et al., Angew. Chem. Int. Ed. 61 (2022) e202114070.
[19] G.R. Genov, H. Takezawa, H. Hayakawa, M. Fujita, J. Am. Chem. Soc. 145 (2023) 17013–17017.
[20] W. Gong, W. Wang, J. Dong, et al., CCS Chem. 5 (2023) 2736–2759.
[21] J. Dong, Y. Liu, Y. Cui, Acc. Chem. Res. 54 (2021) 194–206.
[22] L. Zhang, H. Liu, G. Yuan, Y.F. Han, Chin. J. Chem. 39 (2021) 2273–2286.
[23] D. Didier, B. Tylleman, N. Lambert, et al., Tetrahedron 64 (2008) 6252–6262.
[24] D.L. Jameson, T. Field, M.R. Schmidt, et al., J. Org. Chem. 78 (2013) 11590–11596.
[25] E.O. Bobylev, J. Ruijter, D.A. Poole III, et al., Angew. Chem. Int. Ed. 62 (2023) e202218162.
[26] M. Fujita, D. Oguro, M. Miyazawa, et al., Nature 378 (1995) 469–471.
[27] K. Iizuka, H. Takezawa, M. Fujita, J. Am. Chem. Soc. 145 (2023) 25971–25975.
[28] N. Kishi, Z. Li, K. Yoza, M. Akita, M. Yoshizawa, J. Am. Chem. Soc. 133 (2011) 11438–11441.
[29] M. Shuto, R. Sumida, M. Yuasa, T. Sawada, M. Yoshizawa, JACS Au 3 (2023) 2905–2911.
[30] J.L. Bolliger, A.M. Belenguer, J.R. Nitschke, Angew. Chem. Int. Ed. 52 (2013) 7958–7962.
[31] Y. Yang, T.K. Ronson, J. Zheng, N. Mihara, J.R. Nitschke, Chem 9 (2023) 1–11.
[32] P. Howlader, S. Mondal, S. Ahmed, P.S. Mukherjee, J. Am. Chem. Soc. 142 (2020) 9070–9078.
[33] D. Samanta, S. Mukherjee, Y.P. Patil, P.S. Mukherjee, Chem. Eur. J. 18 (2012) 12322–12329.

[34] C.S. Arribas, O.F. Wendt, A.P. Sundin, et al., Chem. Commun. 46 (2010) 4381–4383.
[35] M. Han, D.M. Engelhard, G.H. Clever, Chem. Soc. Rev. 43 (2014) 1848–1860.
[36] G.H. Clever, P. Punt, Acc. Chem. Res. 50 (2017) 2233–2243.
[37] J.B. Maglic, R. Lavendomme, J. Appl. Crystallogr. 55 (2022) 1033–1044.
[38] S. Pullen, G.H. Clever, Acc. Chem. Res. 51 (2018) 3052–3064.
[39] K. Wu, J. Tessarolo, A. Baksi, G.H. Clever, Angew. Chem. Int. Ed. 61 (2022) e202205725.
[40] C. Bannwarth, E. Caldeweyher, S. Ehlert, et al., WIREs Comput. Mol. Sci. 11 (2021) e1493.
[41] R. Fu, Q.Y. Zhao, H. Han, et al., Angew. Chem. Int. Ed. 62 (2023) e202315990.
[42] Y.L. Lai, J. Su, L.X. Wu, et al., Chin. Chem. Lett. 35 (2024) 108326.